Published OnlineFirst June 21, 2016; DOI: 10.1158/0008-5472.CAN-15-3152

Molecular and Cellular Pathobiology

Cancer Research

Differential Effects of IL6 and Activin A in the Development of Cancer-Associated Cachexia

Justin L. Chen[1,2], Kelly L. Walton[1], Hongwei Qian[2], Timothy D. Colgan[2,3], Adam Hagg[2], Matthew J. Watt[4,5], Craig A. Harrison[1,5,6], and Paul Gregorevic[2,3,7,8]

Abstract

Cachexia is a life-threatening wasting syndrome lacking effective treatment, which arises in many cancer patients. Although ostensibly induced by multiple tumor-produced cytokines (tumorkines), their functional contribution to initiation and progression of this syndrome has proven difficult to determine. In this study, we used adeno-associated viral vectors to elevate circulating levels of the tumorkines IL6 and/or activin A in animals in the absence of tumors as a tactic to evaluate hypothesized roles in cachexia development. Mice with elevated levels of IL6 exhibited 8.1% weight loss after 9 weeks, whereas mice with elevated levels of activin A lost 11% of their body weight. Co-elevation of both tumorkines to levels approximating those observed in cancer cachexia models induced a more rapid and profound body weight loss of 15.4%. Analysis of body composition revealed that activin A primarily triggered loss of lean mass, whereas IL6 was a major mediator of fat loss. Histologic and transcriptional analysis of affected organs/tissues (skeletal muscle, fat, and liver) identified interactions between the activin A and IL6 signaling pathways. For example, IL6 exacerbated the detrimental effects of activin A in skeletal muscle, whereas activin A curbed the IL6-induced acute-phase response in liver. This study presents a useful model to deconstruct cachexia, opening a pathway to determining which tumorkines are best targeted to slow/reverse this devastating condition in cancer patients. *Cancer Res; 76(18); 5372–82. ©2016 AACR.*

Introduction

Cachexia, a systemic wasting syndrome characterized by a progressive loss of skeletal muscle and fat mass (1), is observed in patients with many chronic diseases, including cancer, chronic obstructive pulmonary disease, heart failure, diabetes, and AIDS (2). Up to 80% of patients with advanced cancer suffer from cachexia and as many as 25% of cancer-related mortalities (2 million people globally in 2012) are attributable to cachexia rather than direct tumor burden (3). As treatment options for cachexia are lacking and patients generally receive little more than palliative care, there is a pressing need to identify the mediators of cancer cachexia and develop therapies to treat this debilitating condition.

Two classes of circulating proteins, proinflammatory cytokines and TGFβ family members, have increasingly been linked to the catabolic events that underlie the loss of muscle and adipose tissue in cachexia. Among proinflammatory cytokines, IL6 is arguably the best-characterized mediator of cachexia (4–7). Many cancer types secrete IL6 and increased circulating levels of this cytokine in patients correlate with weight loss and reduced survival (8). Similarly, serum IL6 levels are elevated in most experimental models of cachexia, and blocking IL6 signaling can reduce the rate of cachexia in mice bearing either colon (C26) or uterine (Yumoto) carcinoma cell lines (9, 10). IL6 appears central to the integrative physiology of cancer cachexia, targeting multiple tissues/organs. In white adipose tissue (WAT) of cachectic mice, IL6 signaling through Stat3 (7) plays important roles in lipid mobilization (11) and increased energy expenditure (12). IL6 is also a key mediator of the futile acute-phase response (APR) in liver during cachexia, driving hepatic export protein production at the expense of protein synthesis in peripheral tissue, such as skeletal muscle (5). Whether IL6 directly targets muscle during cachexia, however, is less well defined (13).

In contrast to interleukins, TGFβ family proteins, particularly myostatin, activins, and GDF15, have been strongly linked to muscle wasting during cachexia (14–16). Normally, muscle-derived myostatin and circulating activins act in concert to negatively regulate muscle mass (17), but systemic elevation of these growth factors, either in the presence or absence of tumors, results in marked muscle atrophy and cachexia (14–16). Strikingly, in cancer cachexia models, including C26 tumor-bearing mice, inhibin-deficient mice, and nude mice implanted with human melanoma or ovarian carcinoma xenografts, blockade of the activin/myostatin pathway [via delivery of soluble activin type II receptor (ActRIIB)] reversed muscle wasting and prolonged survival (18). As the positive effects of soluble ActRIIB in C26

[1]Hudson Institute of Medical Research, Clayton, Australia. [2]Baker IDI Heart and Diabetes Institute, Melbourne, Australia. [3]Department of Physiology, The University of Melbourne, Melbourne, Australia. [4]The Obesity and Metabolism Program of the Biomedicine Discovery Institute, Monash University, Clayton, Australia. [5]Department of Physiology, Monash University, Clayton, Australia. [6]Department of Molecular and Translational Sciences, Monash University, Clayton, Australia. [7]Department of Biochemistry and Molecular Biology, Monash University, Clayton, Australia. [8]Department of Neurology, The University of Washington School of Medicine, Seattle, Washington.

Note: Supplementary data for this article are available at Cancer Research Online (http://cancerres.aacrjournals.org/).

C.A. Harrison and P. Gregorevic contributed equally to this article.

Corresponding Author: Paul Gregorevic, Baker IDI Heart and Diabetes Institute, P.O. Box 6492, Melbourne 3004, Australia. Phone: 61385321224; Fax: 61385321100; E-mail: paul.gregorevic@bakeridi.edu.au

doi: 10.1158/0008-5472.CAN-15-3152

Published OnlineFirst June 21, 2016; DOI: 10.1158/0008-5472.CAN-15-3152

mice were observed despite persistently elevated levels of IL6, IL1β, and TNFα (18), the authors speculated that activin-related ligands are more important than proinflammatory cytokines in triggering muscle wasting and cachexia.

Different groups have identified IL6 or activin A as the key mediator of cachexia in the C26 model, supporting the concept that tumors secrete multiple cachectic factors, each of which contribute to systemic wasting (1, 5). However, because different cancer types, and potentially every individual cancer patient, will produce a defined set of tumorkines (1), it has proven extremely difficult to determine the relative contribution of these factors to cachexia progression. In this study, we have evaluated a new approach to identify the factors contributing to cachexia. Using adeno-associated viral vectors (AAV vectors), we elevated circulating IL6 and/or activin A, in the absence of tumor burden, and determined the relative contribution of each factor to the pathogenesis of cachexia.

Materials and Methods

Production of AAV vectors

cDNA constructs encoding for IL6, activin A, TNFα, and Tweak were cloned into an AAV expression plasmid consisting of a CMV promoter/enhancer and SV40 poly-A region flanked by AAV2 terminal repeats. These AAV plasmids were cotransfected with pDGM6 packaging plasmid into human embryonic kidney 293 (HEK293) cells (cell line not authenticated) to generate type-6 pseudotyped viral vectors, which were harvested and purified as described previously (19). The purified vector preparations were quantified with a customized sequence-specific quantitative PCR-based reaction (Life Technologies; ref. 19).

Animal experiments

All experiments were conducted in accordance with the code of practice for the care and use of animals for scientific purposes (National Health & Medical Council of Australia, 2015). Implantation of colon-26 (C26)-derived tumor tissue was carried out on isoflurane-anesthetized male BALB/c mice, as described previously (20). Weighing and body composition was performed using quantitative magnetic resonance (EchoMRI) periodically during the 3-week experiment. At the experimental endpoint, terminal bloods were collected from anesthetized mice by cardiac puncture, and mice were then humanely euthanized via cervical dislocation. Tissues and organs were excised rapidly and weighed before subsequent processing.

For the analysis of IL6, TNFα, and Tweak, AAV6 vectors carrying these transgenes were injected at 10^9, 5×10^9, 10^{10}, 5×10^{10}, or 10^{11} vector genomes (vg) into the right tibialis anterior (TA) muscles of 6- to 8-week-old male C57BL/6 mice under isoflurane anesthesia. Control vectors carrying an empty transgene were injected into the right TA muscles of separate cohorts of mice. For the analysis of activin A and IL6, AAV6 vectors carrying the activin A transgene were injected at a total dose of 1.3×10^{12} vg into the right TA, gastrocnemius, and quadriceps muscles of 30-week-old male C57BL/6 mice under isoflurane anesthesia, whereas IL6 vectors were injected at 7×10^9 vg into the left TA muscle. Control vectors carrying an empty transgene were injected at equivalent doses into the respective muscles of a separate cohort of mice. Weighing and body composition was performed using quantitative magnetic resonance (EchoMRI) weekly during the 9-week experiment. Blood was collected from the tail vein at defined time points throughout the experiment. At the experimental endpoint, all mice were humanely euthanized via cervical dislocation. Tissues and organs were rapidly excised and weighed before subsequent processing.

ELISAs

Activin A was measured using a specific ELISA as previously described (Oxford Bio-Innovations; ref. 21). Serum IL6 concentration was measured using an ELISA Kit according to the manufacturer's specifications (Ray Biotech).

Histology

Harvested muscles, heart, liver, and spleen were placed in OCT cryoprotectant and frozen in liquid nitrogen–cooled isopentane. The frozen samples were cryosectioned at 10-μm thickness and stained with hematoxylin and eosin or Masson's Trichrome, as described previously (14). Harvested adipose tissues were fixed with 4% PFA overnight at 4°C and stored in 70% (w/v) ethanol. The fixed tissues were embedded in paraffin, cut at 5 μm thickness and stained with hematoxylin and eosin. All sections were mounted using DePeX mounting medium (VWR) and imaged at room temperature using a U-TV1X-2 camera mounted to an IX71 microscope, and an Olympus PlanC 10×/0.25 objective lens. DP2-BSW acquisition software (Olympus) and Aperio AT Turbo (Leia Biosystems) used to acquire images. The minimum Feret's diameter of muscle fibers was determined using ImageJ software (NIH) by measuring at least 150 fibers per mouse muscle.

qRT-PCR

Total RNA was collected from TA and quadriceps muscles, liver, and WAT using TRIzol. RNA (1–3 μg) was reverse transcribed using the high capacity RNA-to-cDNA Kit (Life Technologies). Gene expression levels were analyzed by qRT-PCR, with *Hprt* to standardize cDNA concentrations, using Taqman gene expression assays (Life Technologies) and ABI detection software. Data were analyzed using the ΔΔCT method of analysis and normalized to a control value of 1.

Western blotting

TA and quadriceps muscles, heart, liver, spleen, and WAT were homogenized in RIPA-based lysis buffer (Millipore) supplemented with Phosphatase and Protease Inhibitor Cocktails (Sigma Aldrich). Except for WAT, samples were centrifuged at 13,000 × *g* for 15 minutes at 4°C and then denatured for 5 minutes at 95°C. For WAT, protein was precipitated using chloroform–methanol extraction and resuspended in 2% SDS in PBS. Protein concentrations were determined using a Protein Assay Kit (Thermo Scientific). Protein fractions were subsequently separated by SDS-PAGE using pre-cast 4% to 12% Bis-Tris gels (Bio-Rad) blotted onto nitrocellulose membranes (Bio-Rad) and incubated overnight at 4°C with antibodies against pSmad3, Smad3 (Epitomics), LC3A, pStat3, Stat3 (Cell Signaling Technologies) at 1:1,000 dilution, or GAPDH (Santa Cruz Biotechnology) at 1:10,000 as described previously (22), then probed with horseradish peroxidase–conjugated secondary antibody for 1 hour. Chemiluminescence was detected using ECL Western blotting detection reagents (GE Healthcare).

Published OnlineFirst June 21, 2016; DOI: 10.1158/0008-5472.CAN-15-3152

Statistical Analysis

One- and two-way ANOVAs were used to assess statistical differences across conditions, with the Tukey *post hoc* test used for comparisons between the specific group means using GraphPad Prism v.6 (GraphPad). Comparisons between two conditions only utilized the Student *t* test. Data groups with different letters achieved significance of $P < 0.05$. Data are presented as the means ± SEM.

Results

Serum IL6 and activin A levels are elevated in C26 tumor-bearing mice and are associated with decreased tissue/organ mass

In this study, 10-week-old male BALB/c mice began to lose body weight 7 days after implantation of C26 tumors (Fig. 1A). By 18 days post-implantation, tumor-bearing mice had lost greater than 20% of their starting body weight (Fig. 1A). Body composition analysis identified loss of both lean (~12%) and fat (~75%) mass in these mice (Supplementary Fig. S1A and S1B). The reductions in body weight after 18 days were associated with markedly elevated levels of serum IL6 (control: 28.6 ± 32.9 pg/mL, $n = 4$; C26: 2,574 ± 1,664 pg/mL, $n = 6$; Fig. 1B) and activin A (control: 54.4 ± 24.4 pg/mL, $n = 5$; C26: 943.6 ± 481.2 pg/mL, $n = 5$; Fig. 1B).

Reductions in lean mass in mice-bearing C26 tumors were due to significant decreases in the weight of multiple tissues/organs, including skeletal muscle, heart, and liver (Fig. 2A–C; Supplementary Fig. S1C), and occurred despite the spleen more than doubling in size (Fig. 2D). Histologic examination revealed that decreases in muscle mass were a product of muscle fiber atrophy (Fig. 2A), whereas decreases in liver mass may have occurred due to hepatocellular death around the central vein (Fig. 2C; ref. 23). The change in mass of each tissue/organ was associated with enhanced IL6-like signaling, as evident by increased Stat3 phosphorylation (Fig. 2A–D; Supplementary Fig. S1D). In contrast, activation of activin A signaling via p-Smad3 was only apparent in the liver (Fig. 2C), although characteristic changes in the expression of Smad2/3-regulated genes (*Csrp3*, *Igfn1*, and *Ky*; ref. 14) were observed in skeletal muscles of C26 tumor-bearing mice (Supplementary Fig. S1E). Interestingly, significant changes in mRNA levels of IL6 and activin A were observed in some tissues of C26 tumor-bearing mice, which could contribute to the detrimental local effects of these factors (Supplementary Fig. S2A–S2D).

Elevated circulating IL6 and activin A, in the absence of tumor, promotes cachexia

As we have done for activin A (14), we used AAV6 vectors to induce graded increases in circulating IL6 (Supplementary Fig. S3A). Administering a vector dose of 7×10^9 viral genomes in tumor-free mice raised serum IL6 levels to approximately the same extent (90-fold) as observed in C26 tumor-bearing mice (Fig. 1B). A time-course analysis indicated that the secretion of IL-6 from the TA muscle was rapid, with a 22-fold increase in circulating levels by 3 days and a 117-fold increase by 3 weeks (Fig. 3A). Circulating activin A levels rose more gradually (Fig. 3A), but were 4- to 5-fold elevated prior to the initiation of whole body wasting (Fig. 3B).

Thirty-week-old mice injected with control vector lost a small proportion (−3.7%) of their starting body mass over the ensuing 9 weeks (Fig. 3B), whereas mice with elevated levels of IL6 demonstrated more substantial weight loss (−8.1% or −3.0 ± 1.0 g). Consistent with our previous study (14), high circulating activin A induced an ~11% decrease in body mass (−4.0 ± 1.4 g) by 9 weeks after vector administration (Fig. 3B). When serum IL6 and activin A were co-elevated to levels approximating those observed in the C26 cachexia model, mice experienced more rapid and profound (−15.4%; −5.9 ± 1.8 g) weight loss, consistent with these factors exerting an additive (rather than synergistic) net effect (Fig. 3B).

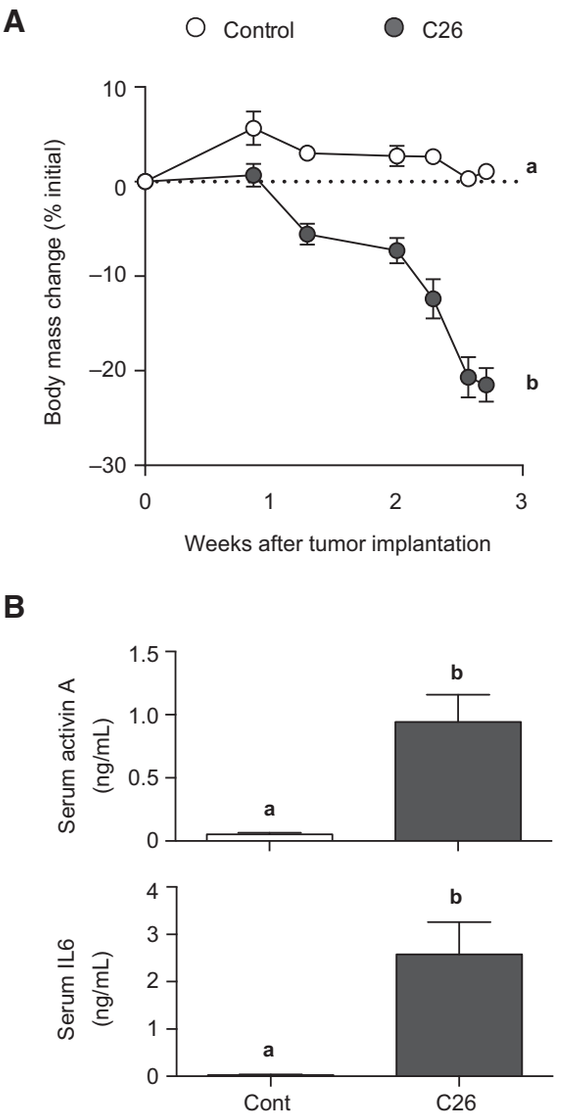

Figure 1.

IL6 and activin A are elevated in the C26 tumor-bearing model of cancer cachexia. Ten-week-old male BALB/c mice were implanted with 1 mm^3 fragments of solid C26 tumor in the flank (control mice received sham surgery). **A,** body weights were measured and plotted as percentage change from week of C26 implantation ($n = 4$–6). **B,** terminal blood samples were collected and activin A and IL6 levels in serum were measured using specific ELISAs ($n = 4$–5). All experiments, unpaired Student *t* test; data groups with different letters achieved significance of $P < 0.05$.

Published OnlineFirst June 21, 2016; DOI: 10.1158/0008-5472.CAN-15-3152

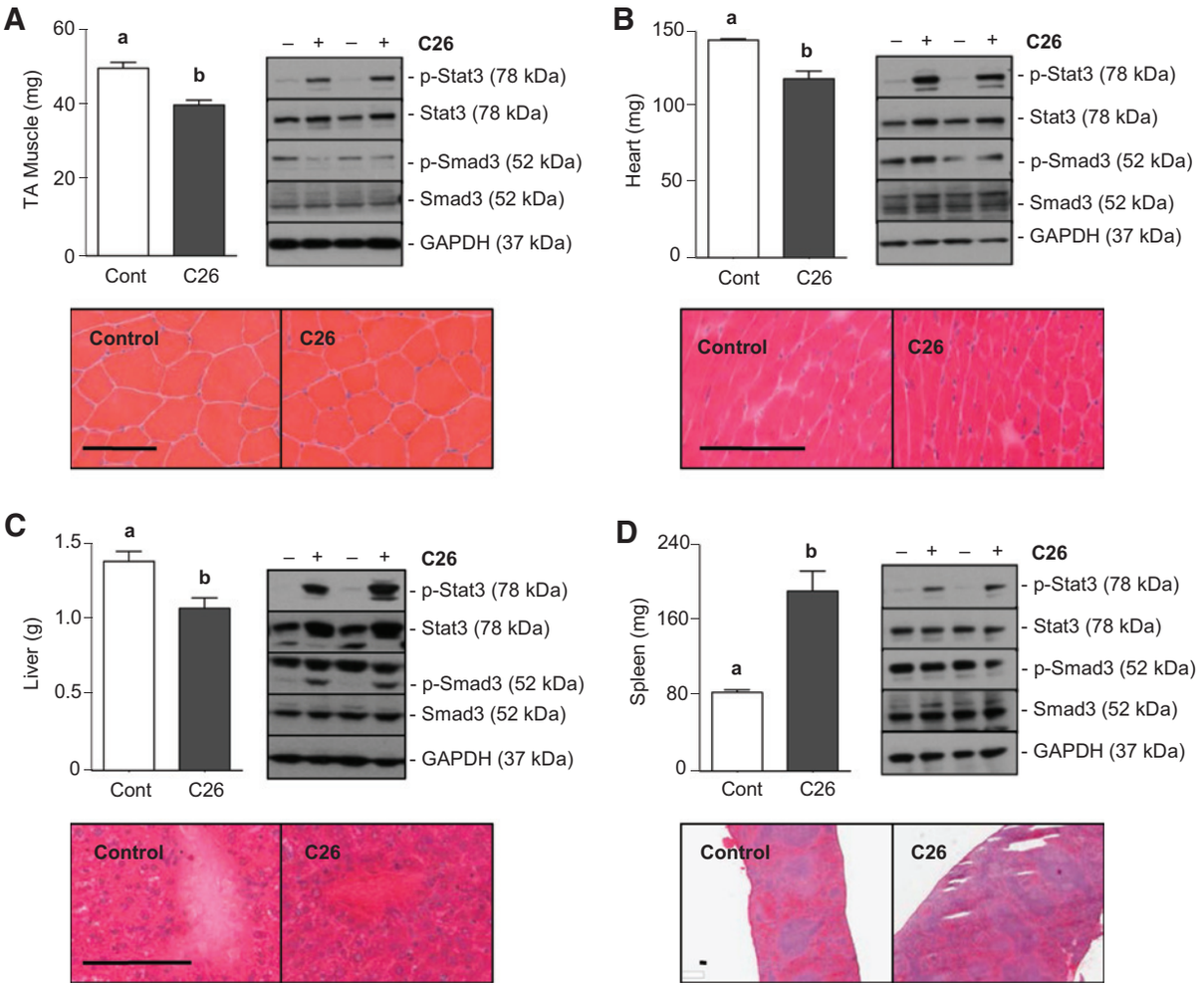

Figure 2.

IL6 and activin A signaling in tissues/organs affected by cachexia in C26 mice. Ten-week-old male BALB/c mice were implanted with 1 mm^3 fragments of solid C26 tumor in the flank (control mice received sham surgery). At the experimental endpoint, TA muscle (**A**), heart (**B**), liver (**C**), and spleen (**D**) were excised and weighed ($n = 4$–5, unpaired Student t test at final time point; data groups with different letters achieved significance of $P < 0.05$), and cryosections were stained with hematoxylin and eosin (bar, 100 μm). The phosphorylation of Stat3 and Smad3, downstream transcription factors of IL6 and activin A, respectively, was assessed by Western blot analysis.

Body composition analysis indicated that activin A and IL6 primarily target distinct tissues during the progression of cachexia. Accordingly, the decrease in lean mass (−11.3%) observed when both factors were elevated was almost entirely consistent with the effects of activin A alone (Fig. 3C). Although co-expression of IL6 increased the rate of activin-induced lean tissue loss, particularly during the first 3 weeks, IL6 by itself did not significantly affect lean mass (Fig. 3C). Indeed, only supraphysiological concentrations of IL6 (>58 ng/mL) led to a decrease in lean mass (Supplementary Fig. S3A and S3B). In contrast, IL6 induced a large decrease in fat mass (−25.5%), which was only marginally enhanced (−30.2%) in the presence of high circulating levels of activin A. Alone, a 16-fold increase in serum activin A induced only moderate fat loss (−11%; Fig. 3D).

As IL6 and activin A are two of the factors elevated in C26 tumor-bearing mice, we repeated the above experiments using AAV6 vectors expressing TNFα or TWEAK. Although TNFα, but not TWEAK, caused significant atrophy in the injected TA muscle (Supplementary Fig. S4A–S4D), neither cytokine induced systemic wasting (Supplementary Fig. S4E–S4G).

Impact of IL6 and activin A on skeletal muscle

In these experiments, the right hindlimb muscles served as a local source of activin A secretion into the systemic circulation. These muscles underwent severe atrophy, which was associated with elevated Smad3 phosphorylation (Fig. 4A and B). More distant muscles (e.g., left quadriceps and gastrocnemius) and other lean tissues (liver and heart) exposed to elevated circulating activin A also showed significant atrophy (Supplementary Fig. S5A and S5B). Although we previously showed that activin A initiated muscle wasting after 7 days by upregulating the expression of the muscle-specific ubiquitin ligases, atrogin-1 and MuRF-1 (14), these effects did not persist over 9 weeks of transgene expression (Supplementary Fig. S6A), even though the

Published OnlineFirst June 21, 2016; DOI: 10.1158/0008-5472.CAN-15-3152

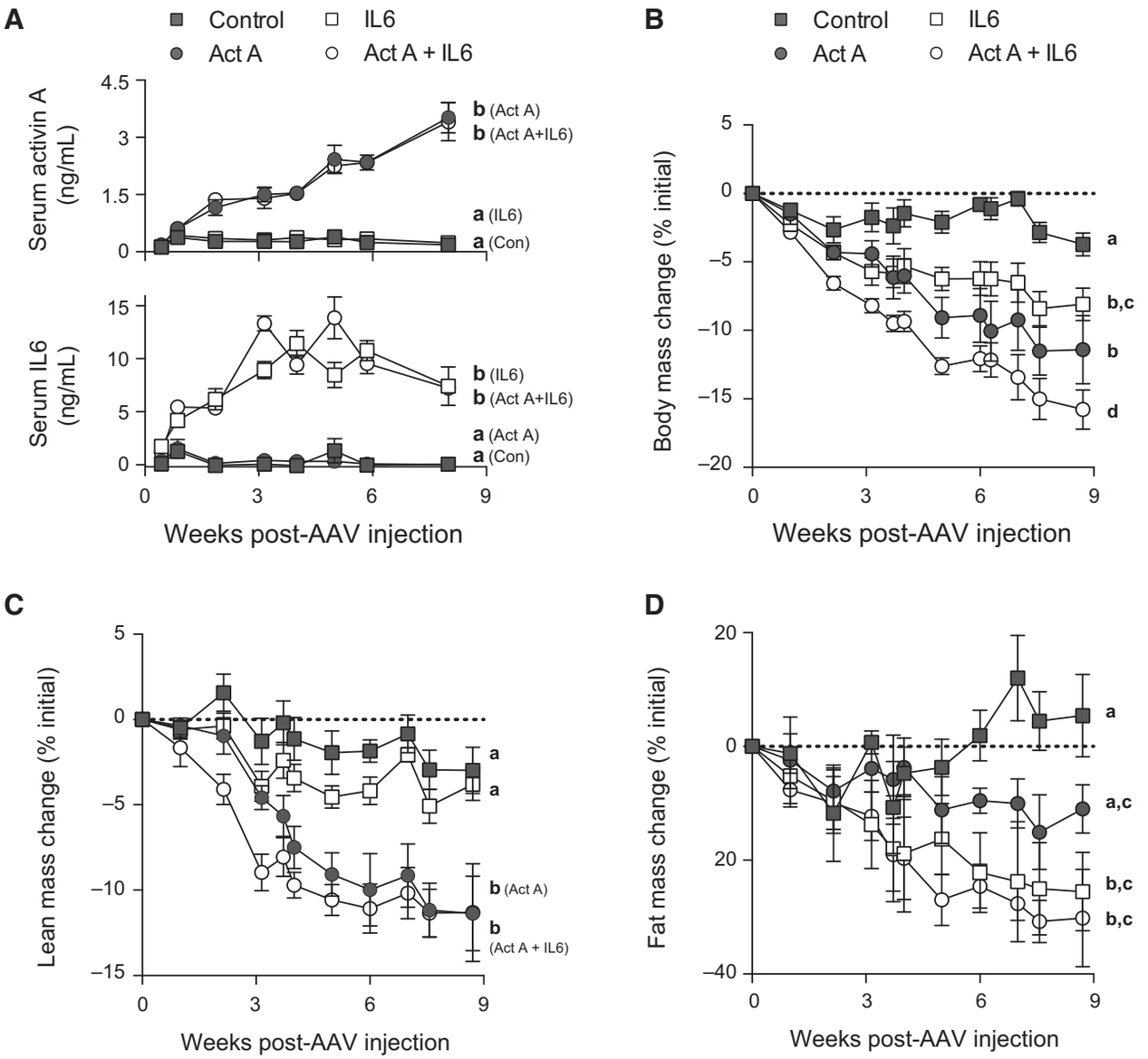

Figure 3.

Elevated circulating IL6 and activin A, in the absence of tumor, promote cachexia. The right hindlimb muscles of 30-week-old C57BL/6 mice were injected with AAV6:activin A (total dose of 1.3×10^{12} vg) and/or the left tibialis anterior muscle was injected with AAV6:IL6 (7×10^{9} vg). Control mice received equivalent doses of AAV6 carrying an empty transgene. **A,** at defined time points after AAV6 injection, bloods were collected and serum levels of activin A and IL6 were determined using specific ELISAs ($n = 3$–5). **B,** during the course of the experiment, body weights were measured and plotted as percentage change from the week of AAV6 injection. Quantitative magnetic resonance was used to measure lean (**C**) and fat (**D**) mass across the experimental time course ($n = 4$–5). All experiments, two-way ANOVA with Tukey *post hoc* test; data groups with different letters at final time point achieved significance of $P < 0.05$.

decline in muscle fiber size was sustained (Fig. 4C and D). The expression of other more recently described ubiquitin ligases, *Mul1* and *Musa1*, also did not change in response to activin A and/or IL6 treatment (Supplementary Fig. S6A). The continued loss of muscle mass may result from the considerable fibrosis that accompanies activin expression within skeletal muscle (Fig. 4E). Another contributing factor may be activation of the autophagy–lysosome pathway, as activin induced a large increase in expression of the autophagy indicator, LC3AI, and its conversion into the phosphatidylethanolamine (PE)-conjugated form, LC3AII (Fig. 4B). Although LC3AII is clearly correlated with the number of autophagosomes, its level at any given time does not necessarily indicate autophagic flux. Therefore, to conclusively demonstrate a role for activin in skeletal muscle autophagy, future experiments would need to measure the amount of LC3AII delivered to lysosomes in the presence or absence of lysosomal protease inhibitors.

IL6, produced by the left TA muscle following injection of AAV6:IL6, had no local or systemic effects on muscle mass (Fig. 4A and Supplementary Fig. S5A), despite activating Stat3 signaling in

Published OnlineFirst June 21, 2016; DOI: 10.1158/0008-5472.CAN-15-3152

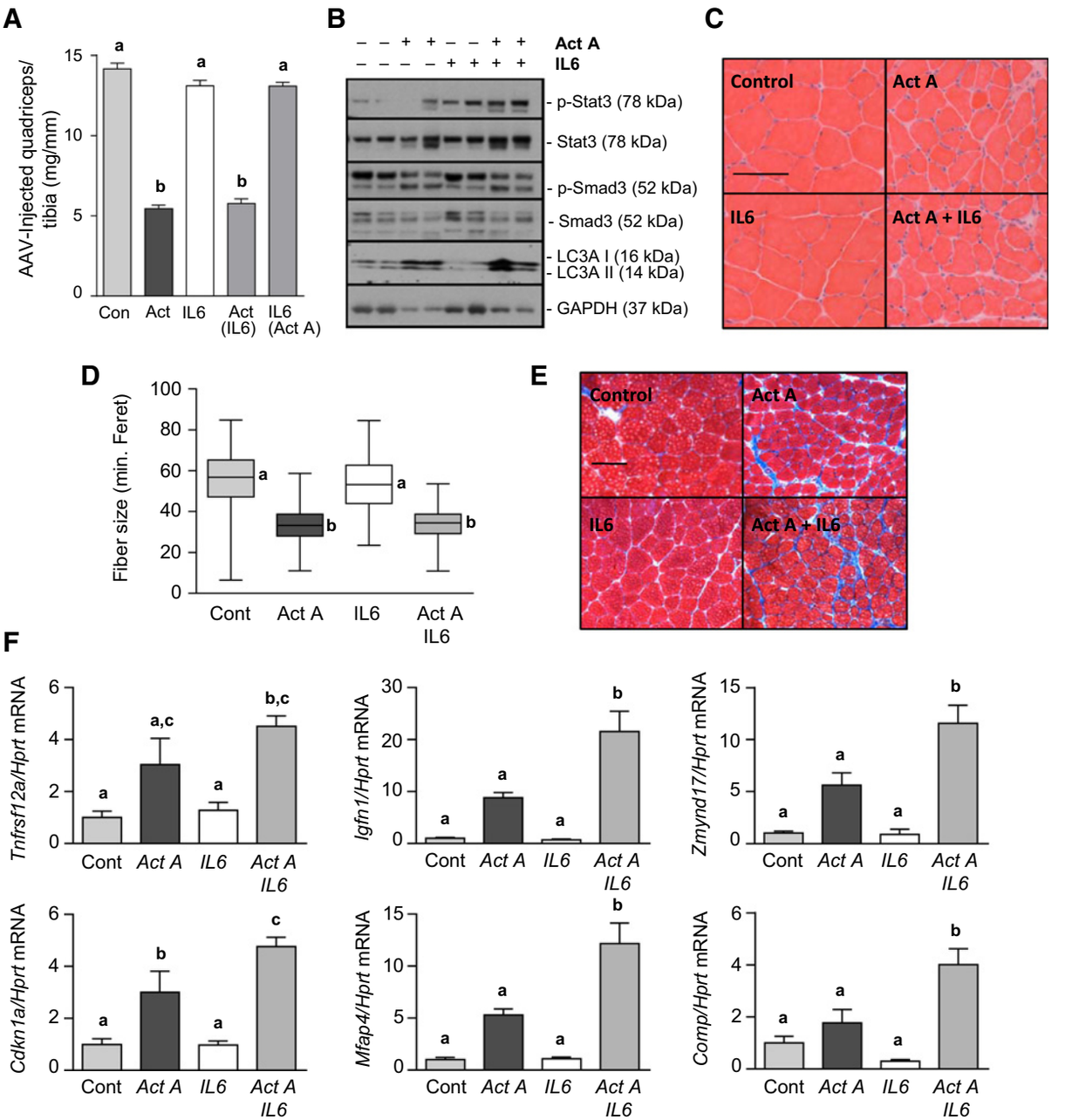

Figure 4.

Interplay between IL6 and activin A in skeletal muscle. **A,** nine weeks after AAV6:activin A and/or AAV6:IL6 injection, right quadriceps muscles were excised and weighed ($n = 10$–11). **B,** the phosphorylation of Stat3 and Smad3, downstream transcription factors for IL6 and activin A, respectively, and the expression of autophagy indicator, LC3AI/LC3AII, was assessed by Western blot analysis. **C,** muscle atrophy in response to activin A and/or IL6 was a product of changes in muscle fiber size (reported here as representative hematoxylin and eosin–stained cryosections; bar, 100 μm), and a box and whisker plot (**D**; $n = 3$ with at least 150 myofibers counted per quadriceps muscle) comprising minimum, lower quartile, median, upper quartile, and maximum values for myofiber diameter. **E,** activin A and/or IL6-induced collagen deposition was assessed using Masson's trichrome stain. **F,** qRT-PCR was performed for activin A–responsive genes in skeletal muscle ($n = 4$–5). All experiments, one-way ANOVA with Tukey *post hoc* test; data groups with different letters achieved significance of $P < 0.05$.

this tissue (Fig. 4B). The lack of an IL6 effect on muscle mass was mirrored by a lack of significant changes in the transcription of IL6 target genes (Supplementary Fig. S6B). Interestingly, at 9 weeks after AAV6:activin A and/or AAV6:IL6 injection, elevated serum IL6 potentiated activin's detrimental effects on skeletal muscle (Fig. 4C–E), increasing the expression of activin-regulated atrophy (*Tnfrsf12a, Igfn1, Zmynd17, Cdkn1a*) and fibrosis (*Mfap4, Comp*) associated genes (Fig. 4F). These data indicate that pathologic levels of IL6 are not sufficient to cause muscle atrophy, but they can enhance the harmful effects of activin A.

Published OnlineFirst June 21, 2016; DOI: 10.1158/0008-5472.CAN-15-3152

IL6 and activin A induce atrophy of WAT

At the experimental endpoint, fat mass was increased by 5.4% from the starting value in mice injected with control vector (Fig. 5A). In contrast, mice demonstrated reduced fat mass relative to starting values, if they had been administered vectors to increase circulating levels of activin A (WAT mass change: $-11.0 \pm 7.4\%$), IL6 ($-25.5 \pm 13.8\%$), or the two factors combined ($-30.2 \pm 17.1\%$; Fig. 5A). Consistent with the observed reductions in WAT mass, there was a corresponding decrease in adipocyte size across the treatment groups (Fig. 5B). Circulating activin A alone increased total and phosphorylated Stat3 levels in WAT (Fig. 5C), suggesting that activin's comparatively modest effects on fat mass may be partially mediated via activation of IL6-like signaling. Conversely, IL6, increased pSmad3 levels (Fig. 5C), thereby identifying WAT as an important site of interaction between these two signaling pathways. At 9 weeks after vector administration, analysis of the expression of genes involved in lipolysis (*Atgl* and *Hsl*), fatty acid oxidation (*Ppara* and *Cpt1a*), and browning (*Prdm16* and *UCP1*) suggested activin A may activate the fatty acid catabolism pathway and, together with IL6, adaptations consistent with browning of WAT (Fig. 5D and Supplementary Fig. S6C and S6D). However, few of these gene changes reached significance. Overall, the relatively minor effects of activin A and IL6 at the gene level in WAT and BAT likely reflects that at 9 weeks, fat loss had essentially stabilized across all groups (Fig. 3D).

Activin A causes necrosis and fibrosis in the liver and suppresses the IL6-induced APR

High levels of circulating activin A have been shown to reduce liver mass (23, 24) and this was replicated in this study (Fig. 6A). In contrast, increased circulating IL6 had no affect on liver mass,

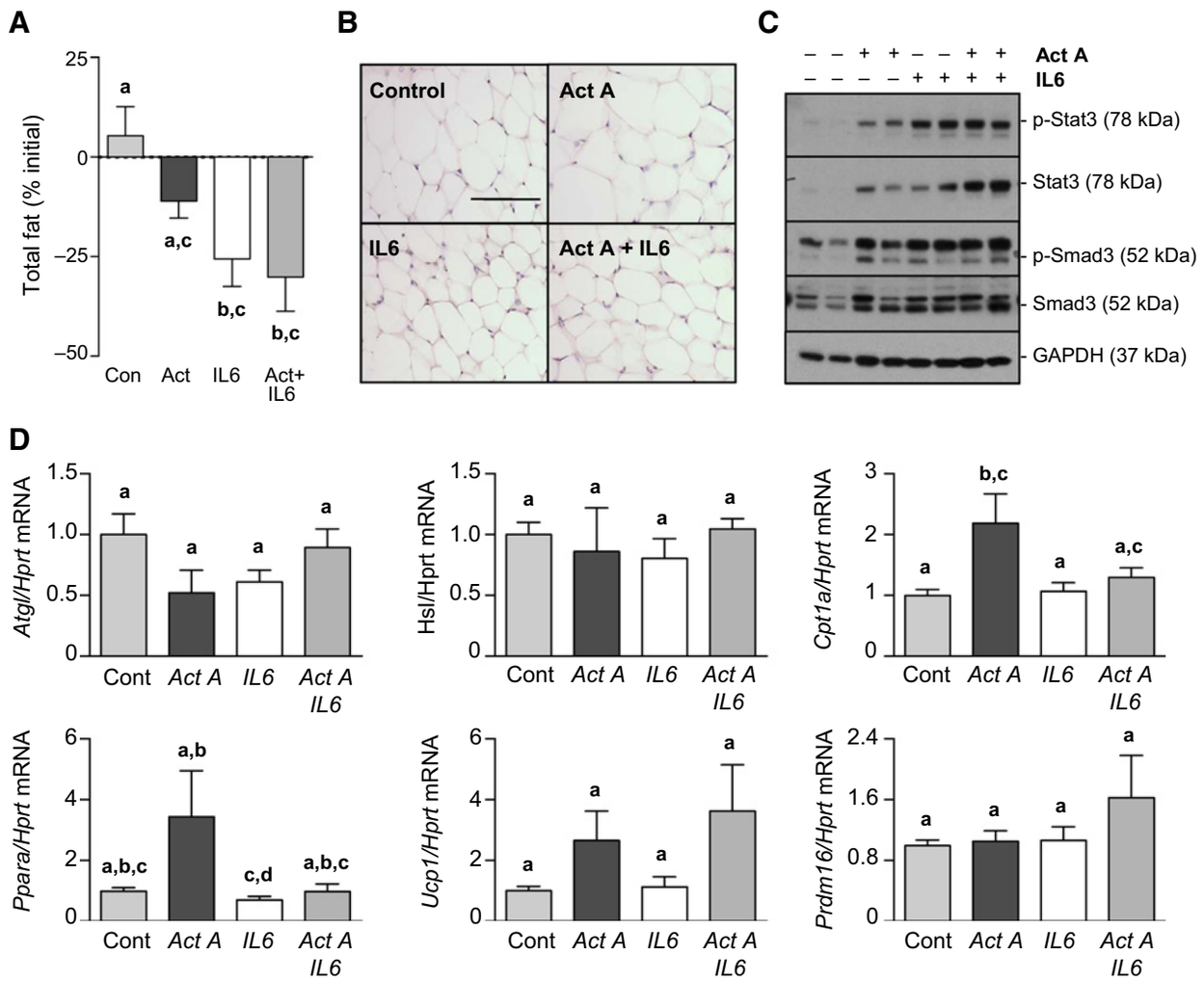

Figure 5.

Interactions between IL6 and activin A in WAT. **A,** nine weeks after AAV6:activin A and/or AAV6:IL6 administration, total fat mass was assessed by EchoMRI and plotted as a percentage of starting fat mass ($n = 4$–5). **B,** epididymal fat was excised, fixed in paraformaldehyde, and sections were stained with hematoxylin and eosin (bar, 100 μm). **C,** the phosphorylation of Stat3 and Smad3, downstream transcription factors of IL6 and activin A, respectively, was assessed by Western blot analysis. **D,** qRT-PCR was performed for activin A- and/or IL6-responsive genes in subcutaneous WAT ($n = 4$–5). All experiments, one-way ANOVA with Tukey *post hoc* test; data groups with different letters achieved significance of $P < 0.05$.

Published OnlineFirst June 21, 2016; DOI: 10.1158/0008-5472.CAN-15-3152

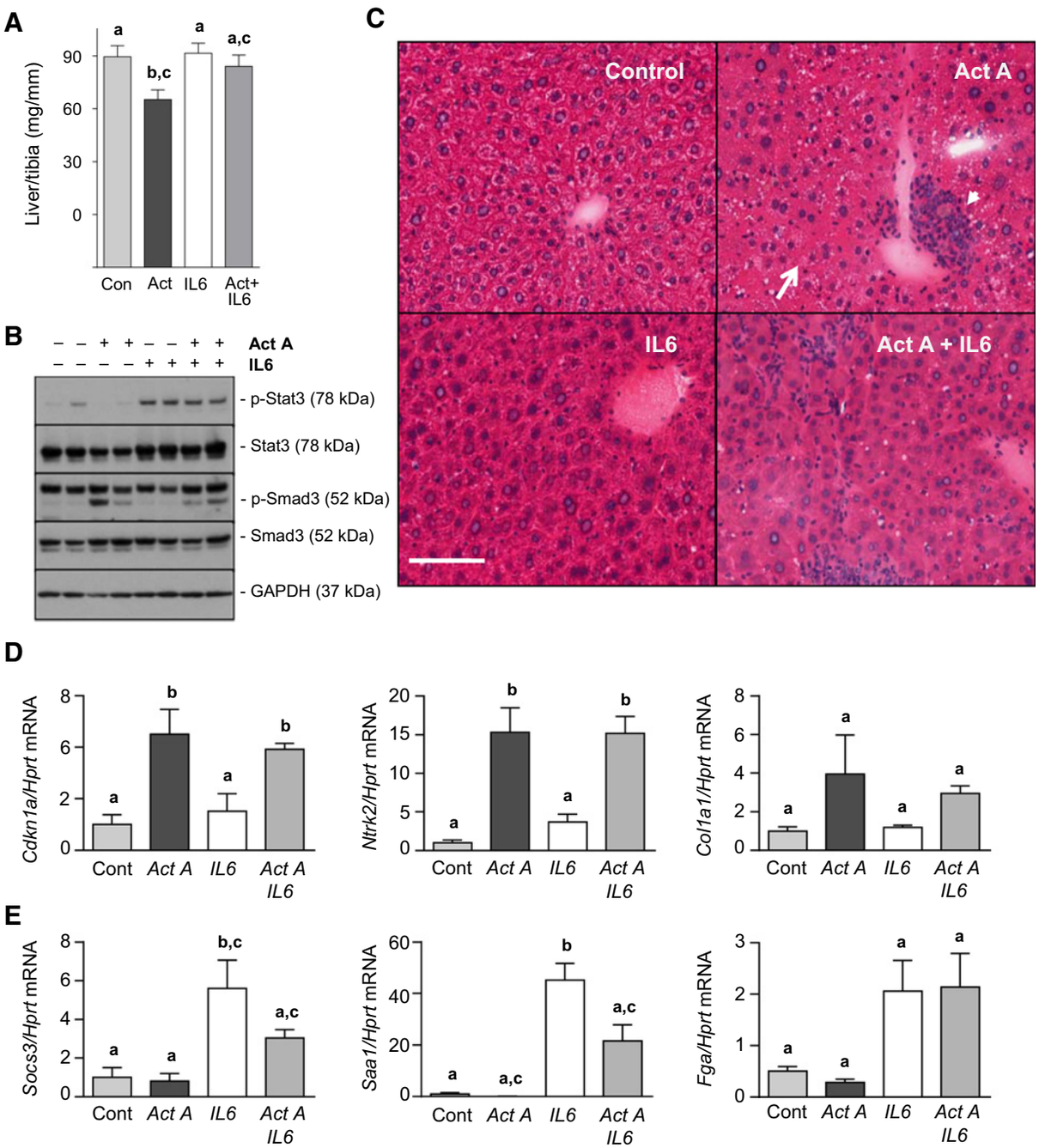

Figure 6.

Elevated circulating IL6 and activin A have profound effects on the liver. **A,** nine weeks after AAV6:activin A and/or AAV6:IL6 injection, livers were excised and weighed ($n = 10$–11). **B,** the phosphorylation of Stat3 and Smad3, downstream transcription factors of IL6 and activin A, respectively, was assessed by Western blot analysis. **C,** cryosections were stained with hematoxylin and eosin and demonstrated hepatocellular necrosis around the central vein (arrow) and foci of chronic lymphocytic inflammation (arrowhead) in mice treated with AAV6:activin A (bar, 100 μm). **D** and **E**, qRT-PCR was performed for activin A- and/or IL6-responsive genes in liver ($n = 4$–5). All experiments, one-way ANOVA with Tukey *post hoc* test; data groups with different letters achieved significance of $P < 0.05$.

despite robustly activating Stat3 in this tissue (Fig. 6B). The livers of mice with high circulating activin A presented with significant hepatocellular necrosis around the central vein and showed foci of chronic lymphocytic inflammation, which were not observed in control mice, or mice with elevated serum IL6 (Fig. 6C). Similar effects have previously been observed in inhibin-deficient mice, which develop gonadal tumors and cachexia subsequent to a significant elevation in circulating activin (23). At the transcript

Published OnlineFirst June 21, 2016; DOI: 10.1158/0008-5472.CAN-15-3152

level, activin A markedly increased expression of the cyclin-dependent kinase inhibitor, Cdkn1a (Fig. 6D), which inhibits mature hepatocyte proliferation (25), and neurotrophic tyrosine kinase receptor type 2 (*Ntrk2*), which plays a role in maintaining innervation of the liver (26). In addition, extracellular matrix (ECM) genes (*Col1a1*, *Col1a3*, *Mfap4*, and *Serpine1*) trended upward in response to activin A (Fig. 6D and Supplementary Fig. S7A) and this effect was associated with substantial collagen deposition throughout the liver (Supplementary Fig. S7B).

A major effect of IL6 during the progression of cancer cachexia is the stimulation of an APR within the liver (5). Consistent with this process, raising circulating IL6 to levels approximating those seen in murine cachexia models induced a substantial increase in the transcription of acute-phase proteins, including serum amyloid A1 (*Saa1*, 51-fold; Fig. 6E). In contrast, high circulating activin A markedly downregulated mRNA levels of *Saa1* (13-fold) when expressed alone, and reduced the IL6-induced APR when both factors were co-elevated in serum (Fig. 6E). These results indicate that IL6 and activin A have potent effects on the liver, which could contribute to the progression of cachexia.

Discussion

Defining how specific tumor-derived cytokines and growth factors contribute to the onset and progression of cachexia has proven challenging against the background of tumor development. For example, mice-bearing C26 tumors have elevated serum levels of IL1β, IL6, TNFα, LIF, oncostatin M, activin A, and activin B (4, 27), each of which has been implicated in the pathogenesis of cachexia. Using recombinant serotype-6 adeno-associated viral vectors (AAV6), we developed a process to raise circulating levels of lead candidate tumorkines in mice in the absence of tumor burden, and examined the role of these factors in the integrative physiology of cachexia. The strength of this approach is its capacity to be adapted to investigate any combination of potential cachectic factors and its applicability to other animal models, such as primates (28).

To demonstrate the utility of this approach, we chose to elevate serum levels of IL6 and activin A, which have each been implicated in cachexia progression in the C26 cancer model (12, 18). We used AAV6 vectors to express IL6 and/or activin A from the left and right hindlimb muscles, respectively, of 30-week-old C57BL/6 mice. In this way, the hindlimb muscles were manipulated to operate as a local source of IL6 and activin A secretion into the systemic circulation. In comparison to the increases in serum IL6 (90-fold) and activin A (17-fold) observed in mice implanted with C26 tumor fragments for 18 days, vector administration to healthy mice for 3 weeks led to a rapid rise in circulating IL6 (117-fold) and a more gradual increase in circulating activin A (4.5-fold, although levels did increase 16-fold after 8 weeks).

Increased circulating activin A levels caused a substantial loss of body weight that was the product of decreases in the mass of skeletal muscle and organs, including the heart and liver. Elevated serum IL6 levels enhanced the initial rate of activin-induced lean tissue loss, but did not have direct effects on lean tissue mass. The lack of an IL6 effect directly on muscle was most vividly demonstrated in the tibialis anterior muscles that had been injected with AAV6:IL6 vectors. These muscles produced high levels of IL6, yet demonstrated no consequential atrophy. Of particular interest when discussing the relative influence of tumorkines alone and in combination, the rate and extent of lean tissue atrophy induced by increased serum levels of IL6 and activin A over 3 weeks were very similar to those observed in mice implanted with cachexia-inducing C26 tumors (Supplementary Fig. S8A). Between 4 and 9 weeks after vector administration, the rate of decline in lean tissue mass in IL6/activin A-treated mice slowed considerably, but ethical guidelines prevented mice bearing C26 tumors from being studied over a similar extended time course. Collectively, the data reported here indicate that elevation of serum activin A, together with contributions from IL6, is capable of recapitulating the rapid loss of lean mass observed in C26 tumor-bearing mice.

Wasting of WAT is another key manifestation of cancer cachexia (3). Inhibiting lipolysis in WAT by genetic ablation of adipose triglyceride lipase ameliorates many features of cachexia, suggesting that loss of fat mass may actually drive the ensuing cachectic phenotype in other tissues (29). In our system, elevated serum IL6 levels triggered a significant decrease in fat mass, which is consistent with previous studies reporting that administration of IL6 increases lipolysis and fatty acid oxidation in mice and humans (7, 11). Interestingly, the rate and extent of fat loss in mice with high circulating IL6 (−25% in 9 weeks) was much reduced compared with that observed in C26 tumor-bearing mice (−74% in 3 weeks; Supplementary Fig. S8B). Thus, IL6 is not sufficient to drive the rapid depletion of adipose tissue during cancer cachexia, although it may play an important role in this process. Other tumorkines that have been implicated in lipid mobilization, such as TNFα or zinc-α2-glycoprotein (3), may be required to exacerbate adipose tissue wasting to the degree observed in cancer-induced cachexia. Our approach is readily amenable to examining the role of these and other prospective tumorkines, alone and in conjunction, in an attempt to replicate the fat loss observed in C26 tumor-bearing mice.

Our tumor-free system allowed us to examine not only the systemic effects of elevated activin A and IL6, but also the interplay of these factors within tissues/organs affected by cancer cachexia. Thus, activin A–induced atrophy and fibrosis in skeletal muscle was enhanced by high serum levels of IL6, despite IL6 having no direct effects on these parameters. Changes in signaling associated with protein synthesis/degradation that we have previously shown underlie early activin-induced muscle wasting (14), were not as evident in muscles examined after 9 weeks of sustained exposure to elevated serum levels of activin A and IL6. Conceivably, the slowing of muscle loss in mice at this time may be accompanied by upregulation of feedback mechanisms that afford muscles a degree of protection from further activin-induced wasting. Similarly modest effects on key processes were observed in WAT where, despite robust Stat3/Smad3 signaling and significant atrophy, only minor changes in genes involved in lipolysis, lipid utilization, and browning were observed after 9 weeks of exposure to high circulating levels of activin A and IL6. Examining tissue samples across a time course that spans disease onset and progression (i.e., when the rate of tissue loss is greatest), may provide additional insights into interactions between these tumorkines and reveal mechanisms that are recruited to slow wasting.

As a key organ in the integrative physiology of cancer cachexia, the liver appears exquisitely sensitive to increased circulating levels of activin A and/or IL6. High serum activin A has been reported to promote cell death in areas surrounding the hepatic central vein (23, 24). In addition to hepatocyte death, we also

observed evidence that circulating activin A can induce fibrosis within the liver, which may constitute a previously unrecognized feature of cancer cachexia. As was seen in skeletal muscle, IL6 enhanced the detrimental effects of activin A in liver, causing increased cell death and fibrosis. In contrast, activin A decreased the IL6-induced APR in the liver, probably by reducing the number of hepatocytes that could respond to this cytokine, rather than directly inhibiting downstream IL6 signaling.

Although our current studies have focused on IL6 and activin A as leading tumorkines, the AAV-based tumor-free methodology that we have developed provides the means to examine the systemic effects of multiple factors and to identify those most important to the initiation and progression of cachexia. For instance, it was recently shown that blocking Fn14, the cognate receptor for the cytokine TWEAK, specifically in the tumors of mice implanted with C26 cells, significantly reduced cancer-induced cachexia and prolonged survival (30). Elsewhere, it has been reported that osteolytic bone metastases promote the release of TGFβ into the circulation, which impairs intracellular Ca^{2+} handling with deleterious consequences for muscle function (31). We propose that the use of AAV vectors to manipulate combinations of tumor- and host-derived factors will help deconstruct the etiology of cachexia. Moreover, this approach could hasten development of cachexia therapeutics, which are urgently required to address the morbidity and mortality associated with many forms of advanced cancer and chronic illness.

Disclosure of Potential Conflicts of Interest

No potential conflicts of interest were disclosed.

Authors' Contributions

Conception and design: J.L. Chen, C.A. Harrison, P. Gregorevic
Development of methodology: J.L. Chen, P. Gregorevic
Acquisition of data (provided animals, acquired and managed patients, provided facilities, etc.): J.L. Chen, K.L. Walton, H. Qian, T.D. Colgan, A. Hagg, M.J. Watt, C.A. Harrison, P. Gregorevic
Analysis and interpretation of data (e.g., statistical analysis, biostatistics, computational analysis): J.L. Chen, K.L. Walton, T.D. Colgan, C.A. Harrison, P. Gregorevic
Writing, review, and/or revision of the manuscript: J.L. Chen, T.D. Colgan, A. Hagg, C.A. Harrison, P. Gregorevic
Administrative, technical, or material support (i.e., reporting or organizing data, constructing databases): J.L. Chen, T.D. Colgan
Study supervision: M.J. Watt, P. Gregorevic

Acknowledgments

The authors thank Prof. Mark Febbraio, Dr. Martin Whitham (Garvan Institute), and Dr. Peter Iliades (Baker IDI Heart and Diabetes Institute) for providing the IL6 transgene, and Dr. Catherine Winbanks (previously Baker IDI Heart and Diabetes Institute) for technical advice and assistance. We also acknowledge the technical assistance of the Histology Facility at Hudson Institute of Medical Research, Monash Histology Platform at Department of Anatomy and Developmental Biology, Monash University, and the Victorian Cancer Biobank.

Grant Support

Grant and Fellowship funding (1078907, 1046782, and 1077703) from the National Health and Medical Research Council (NHMRC) Australia supported C.A. Harrison and P. Gregorevic. J.L. Chen was supported by fellowships from the Cancer Council Victoria and the Endocrine Society Australia. An Early Career Seed Grant from the Victorian Cancer Agency supported K.L. Walton. Hudson Institute of Medical Research and Baker IDI Heart and Diabetes Institute are supported in part by the Operational Infrastructure Support Program of the Victorian Government.

The costs of publication of this article were defrayed in part by the payment of page charges. This article must therefore be hereby marked *advertisement* in accordance with 18 U.S.C. Section 1734 solely to indicate this fact.

Received November 17, 2015; revised June 8, 2016; accepted June 13, 2016; published OnlineFirst June 21, 2016.

References

1. Tsoli M, Robertson G. Cancer cachexia: malignant inflammation, tumorkines, and metabolic mayhem. Trends Endocrinol Metab 2013;24:174–83.
2. Acharyya S, Guttridge DC. Cancer cachexia signaling pathways continue to emerge yet much still points to the proteasome. Clin Cancer Res 2007;13:1356–61.
3. Tisdale MJ. Mechanisms of cancer cachexia. Physiol Rev 2009;89:381–410.
4. Bonetto A, Aydogdu T, Kunzevitzky N, Guttridge DC, Khuri S, Koniaris LG, et al. STAT3 activation in skeletal muscle links muscle wasting and the acute phase response in cancer cachexia. PloS ONE 2011;6:e22538.
5. Fearon KC, Glass DJ, Guttridge DC. Cancer cachexia: mediators, signaling, and metabolic pathways. Cell Metab 2012;16:153–66.
6. Narsale AA, Carson JA. Role of interleukin-6 in cachexia: therapeutic implications. Curr Opin Supp Pall Care 2014;8:321–7.
7. Tsoli M, Schweiger M, Vanniasinghe AS, Painter A, Zechner R, Clarke S, et al. Depletion of white adipose tissue in cancer cachexia syndrome is associated with inflammatory signaling and disrupted circadian regulation. PloS ONE 2014;9:e92966.
8. Moses AG, Maingay J, Sangster K, Fearon KC, Ross JA. Pro-inflammatory cytokine release by peripheral blood mononuclear cells from patients with advanced pancreatic cancer: relationship to acute phase response and survival. Oncol Rep 2009;21:1091–5.
9. Strassmann G, Fong M, Freter CE, Windsor S, D'Alessandro F, Nordan RP. Suramin interferes with interleukin-6 receptor binding in vitro and inhibits colon-26-mediated experimental cancer cachexia in vivo. J Clin Invest 1993;92:2152–9.
10. Tamura S, Ouchi KF, Mori K, Endo M, Matsumoto T, Eda H, et al. Involvement of human interleukin 6 in experimental cachexia induced by a human uterine cervical carcinoma xenograft. Clin Cancer Res 1995;1:1353–8.
11. van Hall G, Steensberg A, Sacchetti M, Fischer C, Keller C, Schjerling P, et al. Interleukin-6 stimulates lipolysis and fat oxidation in humans. J Clin Endocrinol Metab 2003;88:3005–10.
12. Petruzzelli M, Schweiger M, Schreiber R, Campos-Olivas R, Tsoli M, Allen J, et al. A switch from white to brown fat increases energy expenditure in cancer-associated cachexia. Cell Metab 2014;20:433–47.
13. Baltgalvis KA, Berger FG, Pena MM, Davis JM, Muga SJ, Carson JA. Interleukin-6 and cachexia in ApcMin/+ mice. Am J Physiol 2008;294:R393–401.
14. Chen JL, Walton KL, Winbanks CE, Murphy KT, Thomson RE, Makanji Y, et al. Elevated expression of activins promotes muscle wasting and cachexia. FASEB J 2014;28:1711–23.
15. Johnen H, Lin S, Kuffner T, Brown DA, Tsai VW, Bauskin AR, et al. Tumor-induced anorexia and weight loss are mediated by the TGF-beta superfamily cytokine MIC-1. Nature Med 2007;13:1333–40.
16. Zimmers TA, Davies MV, Koniaris LG, Haynes P, Esquela AF, Tomkinson KN, et al. Induction of cachexia in mice by systemically administered myostatin. Science 2002;296:1486–8.
17. Chen JL, Walton KL, Al-Musawi SL, Kelly EK, Qian H, La M, et al. Development of novel activin-targeted therapeutics. Mol Therapy 2015;23:434–44.
18. Zhou X, Wang JL, Lu J, Song Y, Kwak KS, Jiao Q, et al. Reversal of cancer cachexia and muscle wasting by ActRIIB antagonism leads to prolonged survival. Cell 2010;142:531–43.
19. Blankinship MJ, Gregorevic P, Allen JM, Harper SQ, Harper H, Halbert CL, et al. Efficient transduction of skeletal muscle using vectors based on adeno-associated virus serotype 6. Mol Therapy 2004;10:671–8.

Published OnlineFirst June 21, 2016; DOI: 10.1158/0008-5472.CAN-15-3152

20. Aulino P, Berardi E, Cardillo VM, Rizzuto E, Perniconi B, Ramina C, et al. Molecular, cellular and physiological characterization of the cancer cachexia-inducing C26 colon carcinoma in mouse. BMC Cancer 2010;10:363.
21. Knight PG, Muttukrishna S, Groome NP. Development and application of a two-site enzyme immunoassay for the determination of 'total' activin-A concentrations in serum and follicular fluid. J Endocrinol 1996;148:267–79.
22. Winbanks CE, Wang B, Beyer C, Koh P, White L, Kantharidis P, et al. TGF-beta regulates miR-206 and miR-29 to control myogenic differentiation through regulation of HDAC4. J Biol Chem 2011;286:13805–14.
23. Matzuk MM, Finegold MJ, Mather JP, Krummen L, Lu H, Bradley A. Development of cancer cachexia-like syndrome and adrenal tumors in inhibin-deficient mice. Proc Natl Acad Sci U S A 1994;91:8817–21.
24. Schwall RH, Robbins K, Jardieu P, Chang L, Lai C, Terrell TG. Activin induces cell death in hepatocytes in vivo and in vitro. Hepatology 1993;18:347–56.
25. Albrecht JH, Meyer AH, Hu MY. Regulation of cyclin-dependent kinase inhibitor p21(WAF1/Cip1/Sdi1) gene expression in hepatic regeneration. Hepatology 1997;25:557–63.
26. Garcia-Suarez O, Gonzalez-Martinez T, Perez-Perez M, Germana A, Blanco-Gelaz MA, Monjil DF, et al. Expression of the neurotrophin receptor TrkB in the mouse liver. Anat Embryol 2006;211:465–73.
27. Seto DN, Kandarian SC, Jackman RW. A key role for leukemia inhibitory factor in C26 cancer cachexia. J Biol Chem 2015;290:19976–86.
28. Lebherz C, Auricchio A, Maguire AM, Rivera VM, Tang W, Grant RL, et al. Long-term inducible gene expression in the eye via adeno-associated virus gene transfer in nonhuman primates. Hum Gene Therapy 2005;16:178–86.
29. Das SK, Eder S, Schauer S, Diwoky C, Temmel H, Guertl B, et al. Adipose triglyceride lipase contributes to cancer-associated cachexia. Science 2011;333:233–8.
30. Johnston AJ, Murphy KT, Jenkinson L, Laine D, Emmrich K, Faou P, et al. Targeting of Fn14 prevents cancer-induced cachexia and prolongs survival. Cell 2015;162:1365–78.
31. Waning DL, Mohammad KS, Reiken S, Xie W, Andersson DC, John S, et al. Excess TGF-beta mediates muscle weakness associated with bone metastases in mice. Nature Med 2015;21:1262–71.

Cancer Research
The Journal of Cancer Research (1916–1930) | The American Journal of Cancer (1931–1940)

AACR American Association for Cancer Research

Differential Effects of IL6 and Activin A in the Development of Cancer-Associated Cachexia

Justin L. Chen, Kelly L. Walton, Hongwei Qian, et al.

Cancer Res 2016;76:5372-5382. Published OnlineFirst June 21, 2016.